Silver Cluster Interactions with Tyrosine

Subjects: Biochemical Research Methods

Contributor: Andrey Buglak

Tyrosine (Tyr) is involved in the synthesis of neurotransmitters, catecholamines, thyroid hormones, etc. Multiple pathologies are associated with impaired Tyr metabolism. Silver nanoclusters (Ag NCs) can be applied for colorimetric, fluorescent, and surface-enhanced Raman spectroscopy (SERS) detection of Tyr.

tyrosine silver nanoclusters aromatic amino acid detection amino acid complexes with metals binding energy

1. Introduction

Subnanometer metal nanoclusters (NCs) have gained increasing attention in the last decade due to their applicability in biocatalysis, bioimaging, and biosensing. Noble metal NCs possess high biocompatibility, chemical stability, low toxicity, and low photobleaching [1]. This set of properties allows them to be used both in vitro and in vivo. Obviously, it is possible to use Ag NCs for biosensor determination of Tyr in aqueous solutions by colorimetric, luminescent, and surface-enhanced Raman spectroscopy (SERS) methods.

Thus, absorption spectra of the ligand and NC are transformed upon the attachment of metal NCs, which can be used for detection of the complex [2]. The same is true for fluorescence spectra [3][4][5]. When interacting with metals, vibrational and Raman spectra undergo certain changes, usually called chemical enhancement, which is exploited by SERS [6]. These types of detection are widely exploited by biosensors [2][7]. Biosensing surpasses more traditional methods, for example, high-performance liquid chromatography (HPLC), infrared spectroscopy, and bioluminescence, because of its higher selectivity, accuracy, and cost-effectiveness [8][9]. Biosensors for various analytes are in great demand nowadays. Biosensors exploit the unique properties of metal nanoclusters and nanoparticles: sensitivity, chemical stability, low toxicity, low photobleaching, intense luminescence, etc [10].

Tyrosine is formed in vivo through hydroxylation of phenylalanine by the phenylalanine-hydroxylase (PAH) enzyme. The significance of tyrosine biosynthesis is huge since it is one of 20 α-proteinogenic amino acids. Tyrosine is also involved in biosynthesis of DOPA, neurotransmitters, catecholamines (dopamine, adrenaline, norepinephrine), thyroid hormones, melanins, etc. (**Figure 1**) [11][12]. There are a number of pathologies associated with impaired tyrosine metabolism: phenylketonuria, hypothyroidism, tyrosinemia, alkaptonuria, and vitiligo [13]. This means that precise determination of Tyr concentration in biological fluids is extremely important [14].

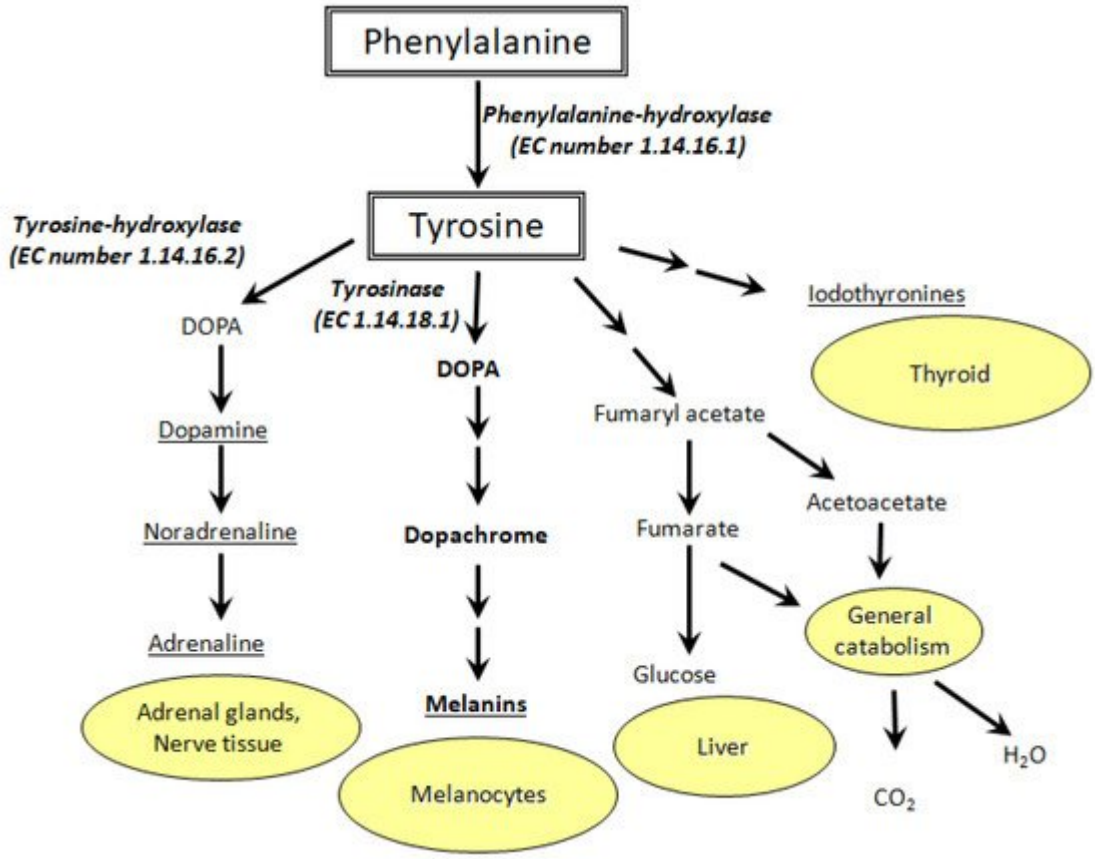

Figure 1. Metabolic pathways of tyrosine oxidation and their biological role (EC stands for enzyme commission).

Vitiligo, for example, is characterized by the appearance of depigmented skin patches. Due to the lack of tyrosinase activity and low 3,4-dioxophenylalanine (DOPA) concentration in melanocytes, melanin synthesis can be disrupted [15]. The etiology of vitiligo is still unknown, but its relationship with the metabolism of aromatic amino acids (Phe, Tyr, DOPA, Trp) is known for certain [16]. Redox reactions of Tyr and DOPA [17][18], as well as their interplay with pterin photoreactions [19][20][21][22][23] are of great importance for melanogenesis and vitiligo etiology/treatment [24][25][26][27][28]. In this regard, biosensors based on metal NCs can be used for cost-effective diagnostics of vitiligo and other Tyr metabolism-related diseases. In particular, silver NCs can help to detect tyrosine in biological fluids and cellular homogenates with high selectivity and sensitivity. We suppose that a cluster should interact with all functional groups of Tyr: amine, carboxyl, and phenol.

Usually, metal NCs are synthesized in solution on biopolymer templates: nucleic acids or proteins [3][29][30]. However, the synthesis is also possible on low molecular weight compounds: thiolates, organophosphates, and amino acids [31]. As is known, Tyr is able to reduce Ag^+ [32]. We have demonstrated that twice deprotonated tyrosine (Tyr^{-2}) can serve as a template for silver NC synthesis in an aqueous solution with an alkaline pH even without the addition of any reducing agent [33]. In this regard, the ability of silver NCs to be synthesized on Tyr can be used for the development of new Ag NC-based Tyr biosensors.

Theoretical studies of amino acid–Ag interactions are not as numerous as they should be. Investigations of silver interactions with histidine [34], glycine, and cysteine [35] were made by Zahra Jamshidi's group; this research mainly

concerned three atomic Ag cluster complexes. Roland Mitric's group conducted a study of silver NC interactions with tryptophan and histidine [36][37]. Our previous studies were mostly about diatomic Ag clusters and a complete set of amino acids [38][39]. Thus, there is a lack of systematic theoretical studies of amino acid interactions with silver clusters of different sizes and charges. Only a theoretical study of cysteine interactions with silver NCs *n* = 2–10 has been published recently [40].

2. Isolated Silver Nanoclusters

First, we analyzed isolated Ag_n^q (*n* = 1–8, q = 0–2) nanoclusters. Ag_2^{2+} has not been realized due to Coulomb repulsion. The Ag–Ag distance is equal to 2.59 Å and 2.72 Å for Ag_2^0 and Ag_2^+, respectively, according to PBE-D3.

Ag_3^q (q = 0, +1, +2) clusters have two types of geometry: linear ($D_{\infty h}$ symmetry) and triangular (D_{3h}). The triangle is the most stable system for q = 0–1, whereas the linear structure is the most energetically favorable for q = +2 (**Figure 2**). Two bonds of the Ag_3^0 NC are 2.67 Å, whereas the third bond equals 2.96 Å. Each bond of the Ag_3^+ cluster is 2.7 Å. Ag_3^{2+} possesses bond lengths equal to 2.84 Å. It should be mentioned that the Ag–Ag bond distance increases with the growth of cluster charge, which is observed for all the clusters with *n* = 2–8.

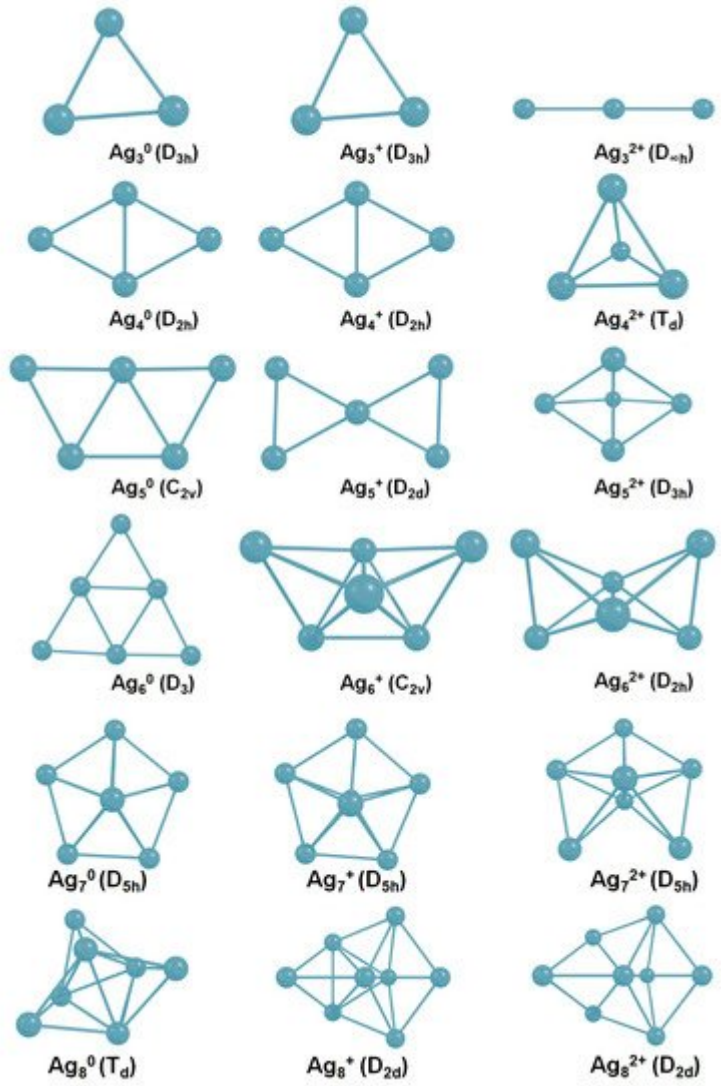

Figure 2. The most stable isomers for isolated Ag_n^q (n = 3–8, q = 0–2) nanoclusters.

Two geometries are the most feasible for the isolated Ag_4^q (q = 0–2) clusters: D_{2h} diamond (Ag_4^0 and Ag_4^+) and T_d tetrahedron (Ag_4^{2+}).

Free Ag_5 clusters have different structures depending on the charge. C_{2v} plane trapezoid is the most favorable form of Ag_5^0. Ag_5^+ is also characterized by plane 2D geometry (D_{2d}). However, the Ag_5^{2+} dicationic cluster possesses a 3D trigonal bipyramid D_{3h} structure (**Figure 2**).

Ag_6 clusters also have different geometries depending on the charge. Isolated Ag_6^0 is a 2D system with a triangular shape (D_3). The most stable isomer of Ag_6^+ is a 3D tetragon pair with a shared bond and an edge (C_{2v} symmetry). The most energetically favorable geometry of Ag_6^{2+} is three-dimensional (D_{2h}).

All Ag_7 NCs possess the same D_{2h} symmetry (**Figure 2**). Apparently, this pentagonal bipyramid structure is very stable for silver NCs, and even the charge does not play a significant role in this case.

Neutral and positively charged Ag_8 NCs have different geometries. The Ag_8^0 cluster, which is often called a magical system [41], possesses T_d geometry. Both Ag_8^+ and Ag_8^{2+} NCs have D_{2d} symmetry.

Therefore, the structure of isolated silver NCs strongly differs depending on the cluster charge. Presumably, clusters can change geometry upon interaction with Tyr. Isolated neutral silver clusters remain two-dimensional with up to six atoms. Ag_n^+ clusters are also subjected to 2D–3D transformation at n = 6. Dicationic Ag_n^{2+} clusters transform from linear to three-dimensional geometry, starting from n = 4. The established results are in agreement with previously reported studies on isolated silver NCs, both theoretical and experimental [42][43][44].

3. Interaction of Ag NCs with Tyrosine

We have performed calculations for the Tyr complexes with silver NCs Ag_n^q (n = 1–8, q = 0–2). Previously, we have shown that silver NCs are most effectively synthesized on tyrosine in an aqueous solution at pH 12.5 [33], which means that the synthesis occurs with the participation of twice deprotonated tyrosine Tyr^{-2}. It is also known that tyrosine can reduce Ag^+, forming a semiquinone (SemiQ) [32]. In this regard, the calculations have been done for three forms of tyrosine: Tyr^{-1}, Tyr^{-2}, and SemiQ. At an alkaline pH, SemiQ is singly deprotonated; for this reason, we have performed calculations for $SemiQ^{-1}$.

We have started the analysis of silver–Tyr interactions by placing Ag atoms near the active sites of Tyr^{-1}. Four sites of Ag attraction have been established: carboxylate (COO^-), hydroxyl, phenyl, and amino group. We have found that the most stable complex is between Ag and COO^-.

Additionally, we have found the atoms responsible for Tyr^{-1} binding with silver ions. We have established five sites of Ag^+ attraction: carboxylate, hydroxyl, phenol ring, amino group (all four are monodentate), carboxylate, and phenol simultaneously (bidentate).

The most stable complex for each Agnq–Tyr-1 system (*n* = 1–8, q = 0–2) is demonstrated in **Figure 3**. Neutral NCs primarily interact with the carboxylate. However, the second site of attraction for Ag20 is the hydroxyl (the premiere Ag–O bond length is 2.17 Å, Ag–H distance is 2.56 Å), and for Ag80 is the amino group (the Ag–O bond length is 2.46 Å, Ag–N distance is 2.34 Å). Additionally, π-interactions are observed for some complexes (for example, in the Ag40–Tyr-1 complex, the distance between Ag and one of the carbon atoms of the phenol is measured to be 2.42 Å). The predominance of Ag–O over Ag–N bonding is not typical for silver cluster complexes of guanine [43] and pterin [45], but is normal for amino acid complexes with silver [33][38].

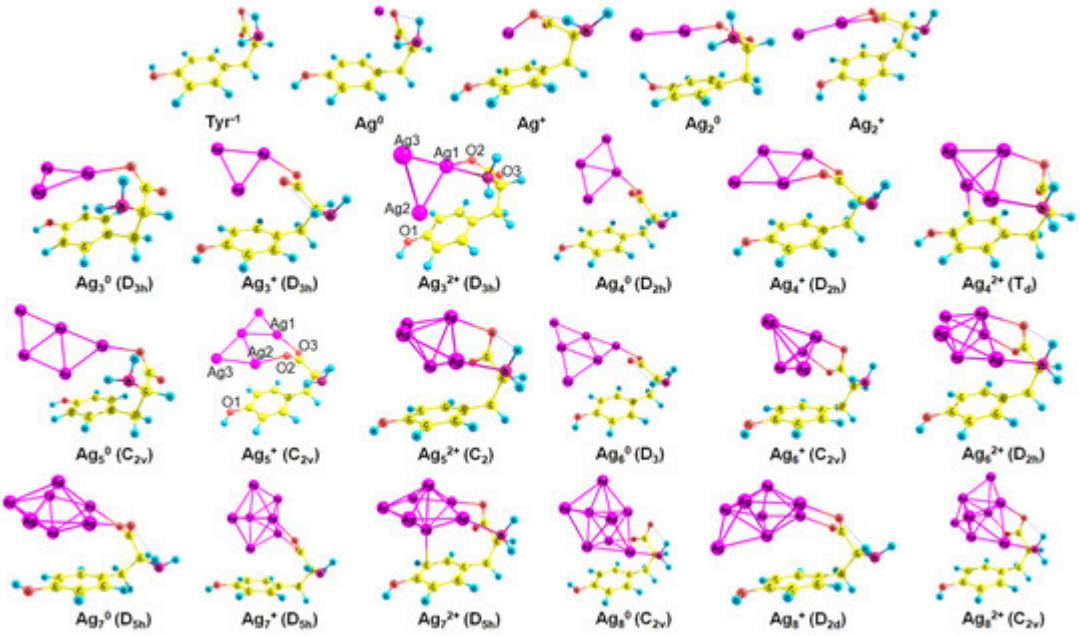

Figure 3. The established complexes of Ag_n^q (*n* = 1–8, q = 0–2) NCs and Tyr^{-1} (PBE-D3 optimization); the point group of a cluster is written in brackets.

For cationic clusters, the COO^- group is also the most favorable for the interaction with Ag NCs (**Figure 3**). In addition, Ag_n^+ clusters reveal π-binding with the phenol ring: to a greater (Ag_7^+: length of Ag–C distance equals 2.42 Å) or lesser extent (Ag_2^+: d(Ag–C) = 2.84 Å). The NH_2 and OH groups are inactive in Ag_n^+ binding with Tyr^{-1}, whereas in the case of the pterin–Ag_n^+ complexes, Ag–N bonding predominates [45].

Tyr^{-1} binds to dicationic NCs like a tridentate chelating agent; it forms bonds with carboxylate, amino group, and phenol. Interactions of Ag with Tyr become more intense since more functional groups are involved in the growth of the cluster charge (**Figure 3**).

In most cases (Ag_4^q, Ag_6^q, Ag_7^q), the cluster geometry does not change upon the interaction with Tyr^{-1}. However, in some cases (Ag_3^{2+}, Ag_5^+, Ag_8^0, and Ag_8^{2+}), it changes significantly (see **Figure 2** and **Figure 3** for comparison). With the attachment of Tyr^{-1}, Ag_3^{2+} alters the geometry from linear ($D_{\infty h}$) to triangular (D_{3h}). Ag_5^+ changes its geometry from D_{2d} to C_{2v} upon the interaction with Tyr^{-1}. Ag_8^0 changes the symmetry point group from T_d to C_{2v}, and Ag_8^{2+} alters geometry from D_{2d} to C_{2v}.

The situation with the geometry of the Tyr^{-2} complexes is similar to that of the Tyr^{-1} systems except that Ag NCs form an additional Ag–O^- bond with the Tyr^{-2} phenol. All clusters have the same symmetry point group, as in the case of the Ag_n^q–Tyr^{-1} complexes.

Regarding $SemiQ^{-1}$ and silver clusters, isolated Ag_8^0 changes the symmetry from T_d to C_s upon the addition of $SemiQ^{-1}$, whereas Ag_8^{2+} changes the geometry from D_{2d} to C_{2v}. As in other cases (Tyr^{-1} and Tyr^{-2}), Ag_3^{2+} changes the geometry from linear to triangular upon the interaction with the ligand. It should be mentioned that $SemiQ^{-1}$ forms Ag–O bonds using the quinone similar to Tyr^{-2} and phenol.

Therefore, the change of cluster geometry during the interplay with Tyr can be used for the experimental detection of Tyr, but generally, the structure of silver NCs does not change significantly with attachment of Tyr^{-1}, Tyr^{-2}, or $SemiQ^{-1}$.

4. Binding Energies

The PBE-D3/6-31G(d,p),LANLTZ method has shown sufficient precision in the estimation of Ag-amino acid binding energy [38]. The PBE-D3/6-31G(d,p) method is also efficiently used for guanine–Ag interactions [46]. For this reason, we have used this approach in our investigation.

We have established the geometry of 66 tyrosine–silver complexes (3 forms of Tyr and 22 nanoclusters). Obviously, the binding energy between Ag NCs and Tyr increases upon H^+ detachment (**Figure 4**); with the increment of Tyr charge from −1 to −2, electrostatic interactions between Ag NCs and Tyr increase. The highest interaction energy is observed for the tyrosine complexes of Ag_3^{2+} NC; the binding energy is equal to −115.1, −122.8, and −146.5 kcal mol^{-1} for $SemiQ^{-1}$, Tyr^{-1}, and Tyr^{-2}, respectively.

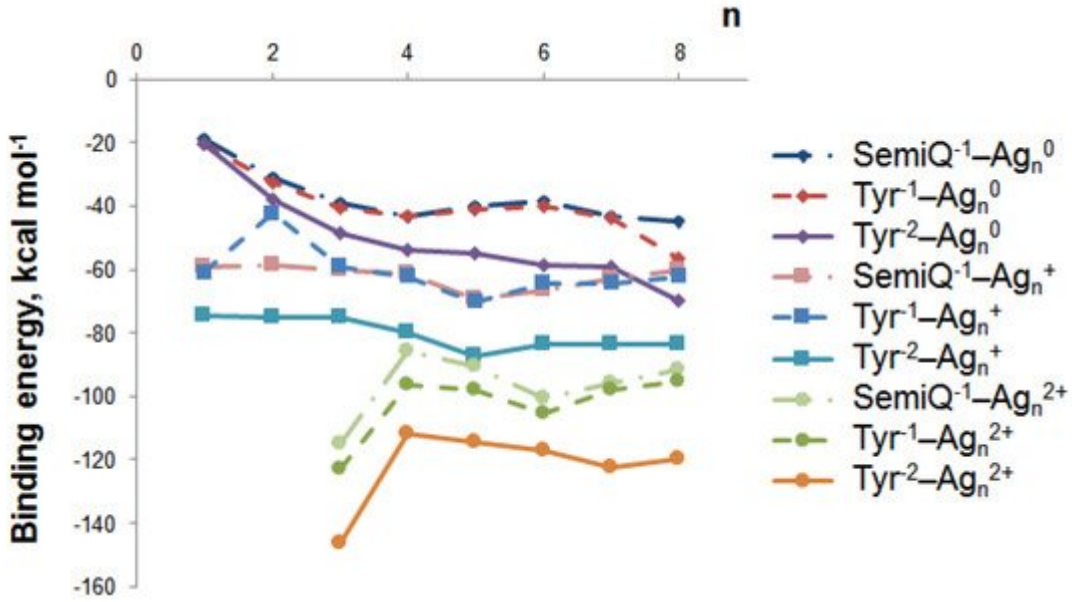

Figure 4. The binding energy between tyrosine and silver nanoclusters Ag_n^q depends on the cluster size (*n*) and charge (q).

Cationic and dicationic silver clusters form much more stable complexes with Tyr^{-1} than the neutral NCs (**Figure 4**), and for this reason, they should be regarded more precisely. The Ag_5^+ cluster is of particular interest due to its highest interaction energy with tyrosine among the clusters with charges of 0 and +1. For $SemiQ^{-1}$, Tyr^{-1}, and Tyr^{-2}, the energy of interaction with Ag_5^+ equals −69.5, −70.2, and −87.3 kcal mol^{-1}, respectively. The binding energies of $SemiQ^{-1}$ and Tyr^{-1} are more or less similar for Ag_n^0 and Ag_n^+ clusters (**Figure 4**).

The increase in the binding energy for the Ag_n^0 systems continues up to the number of atoms equal to 8. Obviously, the most stable Ag_n^0 NC complex with Tyr^{-1} possesses *n*(Ag) > 8. The attachment of Ag_8^0 to Tyr^{-1} (Ag_8^0 changes symmetry from Td to C_{2v}) is characterized by an interaction energy equal to –56.5 kcal mol^{-1}. The biding energies of Ag_8^0 with Tyr^{-2} and $SemiQ^{-1}$ are also the highest among neutral NCs: −69.7 and −44.9 kcal mol^{-1}, respectively.

Therefore, the Ag_3^{2+} cluster possesses the highest binding energy with all three ligands. The Ag_5^+ NC systems are the most stable among clusters, with a charge equal to 0 or +1. The Ag_3^{2+} and Ag_5^+ clusters are the most prospective for experimental synthesis from a theoretical viewpoint and should be regarded as perspective tools for Tyr biosensor development.

References

1. Wan, J.; Zhang, X.; Zhang, K.; Su, Z. Biological nanoscale fluorescent probes: From structure and performance to bioimaging. Rev. Anal. Chem. 2020, 39, 209–221.
2. Tavakkoli Yaraki, M.; Tan, Y.N. Recent advances in metallic nanobiosensors development: Colorimetric, dynamic light scattering and fluorescence detection. Sens. Int. 2020, 1, 100049.
3. Chen, X.; Boero, M.; Lopez-Acevedo, O. Atomic structure and origin of chirality of DNA-stabilized silver clusters. Phys. Rev. Mater. 2020, 4, 065601.
4. Yang, T.-Q.; Peng, B.; Shan, B.-Q.; Zong, Y.-X.; Jiang, J.-G.; Wu, P.; Zhang, K. Origin of the Photoluminescence of Metal Nanoclusters: From Metal-Centered Emission to Ligand-Centered Emission. Nanomaterials 2020, 10, 261.
5. Xiao, Y.; Wu, Z.; Yao, Q.; Xie, J. Luminescent metal nanoclusters: Biosensing strategies and bioimaging applications. Aggregate 2021, 2, 114–132.
6. Shvalya, V.; Filipič, G.; Zavašnik, J.; Abdulhalim, I.; Cvelbar, U. Surface-enhanced Raman spectroscopy for chemical and biological sensing using nanoplasmonics: The relevance of interparticle spacing and surface morphology. Appl. Phys. Rev. 2020, 7, 31307.

7. Romeo, M.V.; López-Martínez, E.; Berganza-Granda, J.; Goñi-de-Cerio, F.; Cortajarena, A.L. Biomarker sensing platforms based on fluorescent metal nanoclusters. Nanoscale Adv. 2021, 3, 1331–1341.
8. Kumar, S.; Dilbaghi, N.; Barnela, M.; Bhanjana, G.; Kumar, R. Biosensors as Novel Platforms for Detection of Food Pathogens and Allergens. Bionanoscience 2012, 2, 196–217.
9. Zhang, R.; Belwal, T.; Li, L.; Lin, X.; Xu, Y.; Luo, Z. Nanomaterial-based biosensors for sensing key foodborne pathogens: Advances from recent decades. Compr. Rev. Food Sci. Food Saf. 2020, 19, 1465–1487.
10. Zeng, Y.; Havenridge, S.; Gharib, M.; Baksi, A.; Weerawardene, K.L.D.M.; Ziefuß, A.R.; Strelow, C.; Rehbock, C.; Mews, A.; Barcikowski, S.; et al. Impact of Ligands on Structural and Optical Properties of Ag 29 Nanoclusters. J. Am. Chem. Soc. 2021, 143, 9405–9414.
11. Fernstrom, J.D.; Fernstrom, M.H. Tyrosine, phenylalanine, and catecholamine synthesis and function in the brain. J. Nutr. 2007, 137, 1539S–1547S.
12. Slominski, A.; Zmijewski, M.A.; Pawelek, J. L-tyrosine and L-dihydroxyphenylalanine as hormone-like regulators of melanocyte functions. Pigment Cell Melanoma Res. 2012, 25, 14–27.
13. Chakrapani, A.; Gissen, P.; McKiernan, P. Disorders of Tyrosine Metabolism BT. In Inborn Metabolic Diseases: Diagnosis and Treatment; Saudubray, J.-M., van den Berghe, G., Walter, J.H., Eds.; Springer: Berlin/Heidelberg, Germany, 2012; pp. 265–276. ISBN 978-3-642-15720-2.
14. Sa, M.; Ying, L.; Tang, A.-G.; Xiao, L.-D.; Ren, Y.-P. Simultaneous determination of tyrosine, tryptophan and 5-hydroxytryptamine in serum of MDD patients by high performance liquid chromatography with fluorescence detection. Clin. Chim. Acta 2012, 413, 973–977.
15. Denat, L.; Kadekaro, A.L.; Marrot, L.; Leachman, S.A.; Abdel-Malek, Z.A. Melanocytes as instigators and victims of oxidative stress. J. Investig. Dermatol. 2014, 134, 1512–1518.
16. Parthasarathy, A.; Cross, P.J.; Dobson, R.C.J.; Adams, L.E.; Savka, M.A.; Hudson, A.O. A Three-Ring Circus: Metabolism of the Three Proteogenic Aromatic Amino Acids and Their Role in the Health of Plants and Animals. Front. Mol. Biosci. 2018, 5, 29.
17. Reid, L.O.; Roman, E.A.; Thomas, A.H.; Dántola, M.L. Photooxidation of Tryptophan and Tyrosine Residues in Human Serum Albumin Sensitized by Pterin: A Model for Globular Protein Photodamage in Skin. Biochemistry 2016, 55, 4777–4786.
18. Neyra Recky, J.R.; Serrano, M.P.; Dántola, M.L.; Lorente, C. Oxidation of tyrosine: Antioxidant mechanism of l-DOPA disclosed. Free Radic. Biol. Med. 2021, 165, 360–367.
19. Castaño, C.; Dántola, M.L.; Oliveros, E.; Thomas, A.H.; Lorente, C. Oxidation of tyrosine photoinduced by pterin in aqueous solution. Photochem. Photobiol. 2013, 89, 1448–1455.

20. Dantola, M.L.; Reid, L.O.; Castaño, C.; Lorente, C.; Oliveros, E.; Thomas, A.H. Photosensitization of peptides and proteins by pterin derivatives. Pteridines 2017, 28, 105–114.
21. Buglak, A.A.; Telegina, T.A. A theoretical study of 5,6,7,8-tetrahydro-6-hydroxymethylpterin: Insight into intrinsic photoreceptor properties of 6-substituted tetrahydropterins. Photochem. Photobiol. Sci. 2019, 18, 516–523.
22. Buglak, A.A.; Telegina, T.A.; Vorotelyak, E.A.; Kononov, A.I. Theoretical study of photoreactions between oxidized pterins and molecular oxygen. J. Photochem. Photobiol. A Chem. 2019, 372, 254–259.
23. Lorente, C.; Serrano, M.P.; Vignoni, M.; Dántola, M.L.; Thomas, A.H. A model to understand type I oxidations of biomolecules photosensitized by pterins. J. Photochem. Photobiol. 2021, 7, 100045.
24. Buglak, A.A.; Telegina, T.A.; Lyudnikova, T.A.; Vechtomova, Y.L.; Kritsky, M.S. Photooxidation of tetrahydrobiopterin under UV irradiation: Possible pathways and mechanisms. Photochem. Photobiol. 2014, 90, 1017–1026.
25. Thomas, A.H.; Zurbano, B.N.; Lorente, C.; Santos, J.; Roman, E.A.; Laura Dántola, M. Chemical changes in bovine serum albumin photoinduced by pterin. J. Photochem. Photobiol. B Biol. 2014, 141, 262–268.
26. Telegina, T.A.; Lyudnikova, T.A.; Buglak, A.A.; Vechtomova, Y.L.; Biryukov, M.V.; Demin, V.V.; Kritsky, M.S. Transformation of 6-tetrahydrobiopterin in aqueous solutions under UV-irradiation. J. Photochem. Photobiol. A Chem. 2018, 354, 155–162.
27. Nizamutdinov, A.; Telegina, T.; Buglak, A.; Lukinova, E.; Madirov, E.; Vechtomova, Y.; Kritsky, M.; Semashko, V. The role of photochemical transformations of tetrahydrobiopterin in the pathogenesis and phototherapy of vitiligo. In Proceedings of the XIV International Conference on Pulsed Lasers and Laser Applications, Tomsk, Russia, 15–20 September 2019; Klimkin, A.V., Tarasenko, V.F., Trigub, M.V., Eds.; SPIE: Bellingham, WA, USA, 2019; Volume 11322, p. 119.
28. Buglak, A.A.; Telegina, T.A.; Vechtomova, Y.L.; Kritsky, M.S. Autoxidation and photooxidation of tetrahydrobiopterin: A theoretical study. Free Radic. Res. 2020, 55, 499–509.
29. Liu, J. DNA-stabilized, fluorescent, metal nanoclusters for biosensor development. TrAC Trends Anal. Chem. 2014, 58, 99–111.
30. Huang, J.; Lin, L.; Sun, D.; Chen, H.; Yang, D.; Li, Q. Bio-inspired synthesis of metal nanomaterials and applications. Chem. Soc. Rev. 2015, 44, 6330–6374.
31. Huang, X.; Li, Z.; Yu, Z.; Deng, X.; Xin, Y. Recent Advances in the Synthesis, Properties, and Biological Applications of Platinum Nanoclusters. J. Nanomater. 2019, 2019, 6248725.
32. Selvakannan, P.R.; Swami, A.; Srisathiyanarayanan, D.; Shirude, P.S.; Pasricha, R.; Mandale, A.B.; Sastry, M. Synthesis of aqueous Au core-Ag shell nanoparticles using tyrosine as a pH-

dependent reducing agent and assembling phase-transferred silver nanoparticles at the air-water interface. Langmuir 2004, 20, 7825–7836.

33. Sych, T.S.; Buglak, A.A.; Reveguk, Z.V.; Pomogaev, V.A.; Ramazanov, R.R.; Kononov, A.I. Which Amino Acids are Capable of Nucleating Fluorescent Silver Clusters in Proteins? J. Phys. Chem. C 2018, 122, 26275–26280.
34. Javan, M.J.; Jamshidi, Z.; Tehrani, Z.A.; Fattahi, A. Interactions of coinage metal clusters with histidine and their effects on histidine acidity; theoretical investigation. Org. Biomol. Chem. 2012, 10, 9373–9382.
35. Pakiari, A.H.; Jamshidi, Z. Interaction of Amino Acids with Gold and Silver Clusters. J. Phys. Chem. A 2007, 111, 4391–4396.
36. Kulesza, A.; Mitrić, R.; Bonačić-Koutecký, V.; Bellina, B.; Compagnon, I.; Broyer, M.; Antoine, R.; Dugourd, P. Doubly charged silver clusters stabilized by tryptophan: Ag42+ as an optical marker for monitoring particle growth. Angew. Chem. Int. Ed. Engl. 2011, 50, 878–881.
37. Sanader, Ž.; Mitrić, R.; Bonačić-Koutecký, V.; Bellina, B.; Antoine, R.; Dugourd, P. The nature of electronic excitations at the metal–bioorganic interface illustrated on histidine–silver hybrids. Phys. Chem. Chem. Phys. 2014, 16, 1257–1261.
38. Buglak, A.A.; Ramazanov, R.R.; Kononov, A.I. Silver cluster–amino acid interactions: A quantum-chemical study. Amino Acids 2019, 51, 855–864.
39. Buglak, A.A.; Kononov, A.I. Comparative study of gold and silver interactions with amino acids and nucleobases. RSC Adv. 2020, 10, 34149–34160.
40. Vu Nhat, P.; Si, N.T.; Tien, N.T.; Nguyen, M.T. Theoretical Study of the Binding of the Thiol-Containing Cysteine Amino Acid to the Silver Surface Using a Cluster Model. J. Phys. Chem. A 2021, 125, 3244–3256.
41. Nhat, P.V.; Si, N.T.; Nguyen, M.T. Elucidation of the molecular and electronic structures of some magic silver clusters Agn (n = 8, 18, 20). J. Mol. Model. 2018, 24, 209.
42. Harb, M.; Rabilloud, F.; Simon, D.; Rydlo, A.; Lecoultre, S.; Conus, F.; Rodrigues, V.; Félix, C. Optical absorption of small silver clusters: Agn, (n = 4–22). J. Chem. Phys. 2008, 129, 194108.
43. Dale, B.B.; Senanayake, R.D.; Aikens, C.M. Research Update: Density functional theory investigation of the interactions of silver nanoclusters with guanine. APL Mater. 2017, 5, 53102.
44. van der Tol, J.; Jia, D.; Li, Y.; Chernyy, V.; Bakker, J.M.; Nguyen, M.T.; Lievens, P.; Janssens, E. Structural assignment of small cationic silver clusters by far-infrared spectroscopy and DFT calculations. Phys. Chem. Chem. Phys. 2017, 19, 19360–19368.
45. Buglak, A.; Kononov, A. Computational study of interactions between silver nanoclusters and pterin. In Proceedings of the FEBS Open Bio, Ljubljana, Slovenia, 3–8 July 2021; Volume 11, pp.

103–507.

46. Chen, X.; Makkonen, E.; Golze, D.; Lopez-Acevedo, O. Silver-Stabilized Guanine Duplex: Structural and Optical Properties. J. Phys. Chem. Lett. 2018, 9, 4789–4794.